Structural Properties of a Model System with Effective Interparticle Interaction Potential Applicable in Modeling of Complex Fluids

ARTICLE *in* THE JOURNAL OF PHYSICAL CHEMISTRY B · NOVEMBER 2008

Impact Factor: 3.3 · DOI: 10.1021/jp804852y · Source: PubMed

2 AUTHORS:

Shiqi Zhou
Central South University
43 PUBLICATIONS **623** CITATIONS
SEE PROFILE

Andrej Jamnik
University of Ljubljana
45 PUBLICATIONS **733** CITATIONS
SEE PROFILE

Structural Properties of a Model System with Effective Interparticle Interaction Potential Applicable in Modeling of Complex Fluids

Shiqi Zhou*

School of Physics Science and Technology, Central South University, Changsha, Hunan, China, 410083

Andrej Jamnik

Faculty of Chemistry and Chemical Technology, University of Ljubljana, Aškerčeva 5, SI-1001 Ljubljana, Slovenia

Received: June 2, 2008; Revised Manuscript Received: August 10, 2008

We report grand canonical ensemble Monte Carlo (MC) simulation and theoretical studies of the structural properties of a model system described by an effective interparticle interaction potential, which incorporates basic interaction terms used in modeling of various complex fluids composed of mesoscopic particles dispersed in a solvent bath. The MC results for the bulk radial distribution function are employed to test the validity of the hard-sphere bridge function in combination with a modified hypernetted chain approximation (MHNC) in closing the Ornstein−Zernike (OZ) integral equation, while the MC data for the density profiles in different inhomogeneous environments are used to assess the validity of the third-order + second-order perturbation density functional theory (DFT). We found satisfactory agreement between the results predicted by the pure theories and simulation data, which classifies the proposed theoretical approaches as convenient tools for the investigation of complex fluids. The present investigation indicates that the bridge function approximation and density functional approximation, which are traditionally used for the study of neutral atomic fluids, also perform well for complex fluids only on condition that the underlying effective potentials include a highly repulsive core as an ingredient.

1. Introduction

The central goal of statistical mechanics[1] is to predict the microscopic structure and macroscopic thermodynamic properties of different model systems from the knowledge of pair potentials prescribed for the interactions between the particles composing the systems under consideration. For simple single-component atomic fluids, this goal can actually be realized as the constituent particles of the neutral atomic fluids interact through spherically symmetrical, e.g., Lennard-Jones (LJ) potential. Structure and thermodynamics of such simple fluids can be therefore predicted very accurately by the statistical mechanical methods, e.g., by the Ornstein−Zernike (OZ) integral equation theory for the homogeneous (bulk) phase,[2] classical density functional theory (DFT) for the inhomogeneous (nonuniform) case,[3] and thermodynamic perturbation theory[4,5] for uniform fluids and solid phases. Statistical mechanical theories are also qualified for the study of binary or ternary mixtures but only on condition that the asymmetries in the charge, size, and interaction energy between the particles of individual components are within 1 order of magnitude.[6] However, the phenomena occurring in everyday life most usually concern the so-called complex fluids[7] involving the multicomponent systems composed of mesoscopic particles dispersed in a solvent of microscopic (atomic) particles, which may contain also other small constituents such as ions of a dissociated salt or short polymeric chains. The size of the bigger colloidal particles exceeds that of the remaining constituents by 3 or 4 orders of magnitude. Theoretical investigations of the modeled complex fluids, which would include detailed information on the length and energy parameters, following from the explicit consideration of internal degrees of freedom of mesoscopic particles are actually not possible. Fortunately, we can capture the essential properties of complicated systems using simplified models with the intermolecular potentials that do not treat all the ingredients on the same footing. It is natural to integrate out in the partition function the coordinates and momenta of the smaller particles[8] leading to an "effective" Hamiltonian, which, together with the direct pair interactions, dominates the structure and thermodynamic behavior of the original complex fluids. Such effective potentials can be of various types and are complicated functions of the properties of the solvent bath. Their shape, range, and strength depend on the size of the solvent particles, solvent−solvent interaction potential, number of components, position of the state point in the phase diagram, etc.[9] Although the derivation of effective potentials represents a rather complicated problem, the fundamental properties of the effective potentials based on numerous theoretical and simulation studies are well-known. It has been indicated that the resulting potential functions are usually one of the following types: short-ranged,[10] oscillatory decaying,[11,12] purely repulsive or purely attractive,[13] alternating between repulsion and attraction,[14,15] or any combination of these features. As the traditional LJ potential is long-ranged, it only suffices for the description of the interparticle interactions in neutral atomic fluids. Although the generalized LJ potential and the hard core attractive Yukawa (HCAY) model can be short-ranged by adjusting the potential parameters, the attractive tails of these potentials are still monotonously decaying function of the interparticle separation. Thus, numerous details characteristic for the effective potentials are not incorporated in these two

* Corresponding author.

10.1021/jp804852y CCC: $40.75
Published on Web 10/09/2008

traditional potential functions. Consequently, the generalized LJ potential and the HCAY potential are only rarely directly applicable for the description of complex fluids. While the single-component OZ integral equation and classical DFT theories are well-established methods for the study of the simple fluids with underlying "normal" potentials consisting of hard core repulsion and attractive tail, their validity for the investigation of these complicated effective potentials has never been assessed. Such test is very important as one of the aims of constructing the effective potentials is to make the single-component statistical mechanics theories applicable for the study of complex fluids whose mesoscopic particles interact through the effective potentials that combine the pure intercolloidal interaction and the excess potential of mean force, which embodies the contributions of solvent molecules to the overall interaction between colloidal particles. Thus, the valid single-component statistical mechanical theories represent natural and unavoidable links for the implementation of the single-component macro-fluid approximations on the complex fluids. As the mathematical forms of the effective potentials are constantly changing, such tests have to be implemented step by step. In the present paper, we investigate the properties of the sample effective potential incorporating an oscillatory decaying tail alternating between repulsive and attractive interaction. In section 2 this effective potential is defined and the methods used for the structural investigation are described. We briefly outline the simulation method and describe the bridge function approximation for closing the OZ integral equation and the third-order + second-order perturbation DFT applied for the determination of the homogeneous and inhomogeneous structures of the model fluid, respectively. Performances of the theoretical approaches are assessed in section 3, which contains the numerical results for the structure at several sets of the model parameters. Finally, some conclusions are given in the last section 4.

2. Model and Methods

2.1. Model. In the present work, the interactions between the particles are represented by a truncated and shifted effective potential with energy parameter ε, hard core diameter σ, and truncation distance r_c:

$$u_{ts}(r) = \begin{cases} \infty & r < \sigma \\ u(r) - u(r_c) & \sigma \le r < r_c \\ 0 & r \ge r_c \end{cases} \quad (1)$$

with

$$u(r)/\varepsilon = \begin{cases} \infty & r < \sigma \\ (\varepsilon_b + 1)(r/\sigma - 1)/(b-1) - 1 & \sigma \le r \le b\sigma \\ \varepsilon_b \exp\left(-\alpha\left(\frac{r}{\sigma} - b\right)\right)\cos\left[k_s\left(\frac{r}{\sigma} - b\right)\right]/\left(\frac{r}{b\sigma}\right)^n & b\sigma < r \end{cases} \quad (2)$$

where the truncation distance r_c is fixed at 4σ. This rather complex potential function is presented in Figure 1. The infinite repulsive potential in eq 2 for the distances $r < \sigma$ represents the prohibition of the hard core overlap originating physically from the strong repulsion of the outer-electron shells occurring in each kind of matter. The last term referring to the distances $r > b\sigma$ has a form similar to that expected for the effective interaction between metal ions screened by the electrons.[16,17] In this case, the potential function has a form of Freidel oscillations with wave vector k_s, where $k_s/2$ corresponds to the wave vector at the Fermi level. The intermediate term for the interparticle distances $\sigma \le r \le b\sigma$ can be regarded as a continuous function with a quarter of an oscillatory circle. It represents the depletion potential[18−21] acting between two large colloidal particles immersed in a bath of small molecules of the solvent, where the solvent−colloid interactions are purely repulsive. Although the depletion potential near the contact region is not simply a term linear in r,[18,19] it is very similar to the linear approximation used in the present study. Particularly, other various approximate depletion potentials such as the well-known AO potential of Asakura and Oosawa,[20] or those based on classical Derjaguin approximation, scaled particle theory, or free volume considerations,[21] are all approximately linear functions of r, as shown in the work of ref 19. For this reason, in the present calculations we simply employ the linear approximation for the depletion potential near the contact region. Hence this sample potential can also represent effective interactions between the colloidal (solute) particles dispersed in a sea of small solvent molecules. In fact, effective potentials for such systems actually show oscillatory tail alternating between the repulsion and attraction.[14,15] The potential is precisely defined by the parameters b, α, k_s, n, and ε_b, which are connected with the properties of the solvent bath by means of very complicated relationships whose explicit mathematical form is beyond the scope of the present paper. The motivation of the present study is to test whether the theoretical approaches established for the ordinary neutral atomic fluids interacting through spherically symmetrical Lennard-Jones (LJ) like potentials perform well also for these effective potentials. In fact, the general relationships between effective potentials and the properties of the solvent bath have not been established yet. What is known are only the main and basic properties the effective potentials generally should hold as described above.

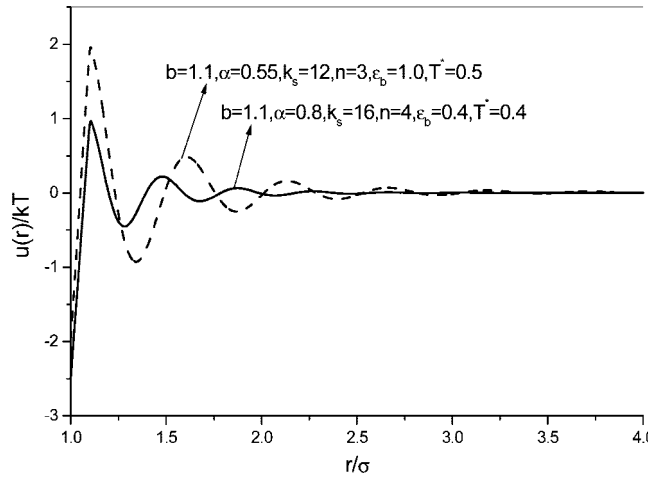

Figure 1. Effective pair potential at two sets of model parameters: (I) $b = 1.1$, $\alpha = 0.55$, $k_s = 12$, $n = 3$, $\varepsilon_b = 1.0$, at the reduced temperature $T^* = 0.5$, and (II) $b = 1.1$, $\alpha = 0.8$, $k_s = 16$, $n = 4$, $\varepsilon_b = 0.4$, at the reduced temperature $T^* = 0.4$.

Both the well-established bridge function approximation for the Ornstein−Zernike (OZ) integral equation and density functional approximation for the excess Helmholtz free energy or its first-order functional derivative have been derived for the potentials used for the modeling of atomic fluids. The usual interatomic potentials consist of the hard core repulsion and monotonously decaying attractive (tail) interaction, the typical examples of such models being the LJ and the HCAY potentials. These models, of course, fail to describe the intermolecular interactions in complex fluids, and, accordingly, they considerably differ from the effective potentials constructed for the

description of complex systems. As the potential applied in the present study incorporates many necessary features of the effective potentials relevant for the description of the interactions between metal ions and depletion interaction in asymmetrical multicomponent systems, it is suitable as a sample model for the test of the single-component statistical mechanical theories. The present sample potential includes many parameters, which, on the one hand, makes possible the potential function to be adjusted to various shapes strongly differing from the "normal" atomic models, thus giving the possibility for a harsh test of the theories, and on the other hand, they capture the influence of the solvent for a variety of different situations.

The major part of the present study is devoted to the investigation of the inhomogeneous structure of the fluid caused by various external fields imposed by different spatial constraints. Besides the single hard wall, we treat also a spherical cavity surrounded by the spherical hard wall, a planar gap, i.e., the two hard walls separated by a distance L, and a hard spherical particle, the corresponding external potentials ϕ_{ext} read

$$\phi_{ext}(z) = \begin{cases} 0 & z > \frac{1}{2}\sigma \\ \infty & \text{otherwise} \end{cases} \tag{3}$$

for a single hard wall

$$\phi_{ext}(r) = \begin{cases} 0 & r < R - \frac{1}{2}\sigma \\ \infty & \text{otherwise} \end{cases} \tag{4}$$

for a spherical cavity with hard spherical wall of radius R,

$$\phi_{ext}(z) = \begin{cases} 0 & \frac{1}{2}\sigma < z < L - \frac{1}{2}\sigma \\ \infty & \text{otherwise} \end{cases} \tag{5}$$

for a planar slit with two plane hard walls situated at $z = 0$ and $z = L$, respectively, and

$$\phi_{ext}(r) = \begin{cases} 0 & r > \frac{1}{2}(D + \sigma) \\ \infty & \text{otherwise} \end{cases} \tag{6}$$

for a hard spherical particle of diameter D.

2.2. Open Ensemble Simulation. Monte Carlo simulations were performed within the grand canonical ensemble using the Metropolis[22] simulation technique. In the open ensemble, the chemical potential μ, the volume V, and the temperature T of the system are fixed, while the number of particles N is allowed to fluctuate. This set of independent parameters that define the thermodynamic state of the system makes possible the study of equilibrium between the fluid in the homogeneous phase and the same fluid being subjected to some external field, which cause the spatial inhomogeneity in the structure of the fluid. This inhomogeneous structure we first determined for the simplest and quite usual geometry considered in theoretical studies of confined fluids that is the one of a planar slit consisting of two parallel, perfectly smooth hard walls at a specified separation L. The actual distance accessible for the fluid was therefore $L - \sigma$. Denoting the perpendicular direction by z, the fluid between the walls extended to infinity along the directions x and y, parallel to the walls. In practical simulations, the system was modeled as an infinite array of identical simulation cells of the volume $L \times a^2$, repeating themselves in the two lateral directions, along which the minimum image convention was applied. No periodicity needed to be assumed in the direction z normal to the plates. In addition, when modeling wide enough pores, where there exist domains of the fluid sufficiently distant from both walls to retain practically nonperturbed density and other properties of the bulk phase, it could be accepted that the structure of the fluid at either plate did not appear to be affected by the presence of the opposite wall. These results should therefore be almost identical to the density profiles next to isolated walls or walls at infinite separations. This way, the structure of the fluid near a hard, flat interface was considered. In most cases, the value for the width of the gap $L = 20\sigma$ was sufficient to avoid the interference between the symmetrical density profiles at individual walls of the pore. Further external field that we considered was imposed by the presence of the closed spherical surface mimicking a spherical cavity of the radius R. In this case, as the MC cell was a closed pool of the fluid, there was no need in using the periodic boundary conditions. Finally, we turned some attention to the structure of the fluid near a single hard sphere. For this system, similarly as in the case of simulation of homogeneous (bulk) phase, the MC cell was a cubic box of the volume a^3 with the periodic boundary conditions imposed in all three directions. The fluid surrounded a hard sphere located at the center of the cell.

During the simulation, the phase space was sampled through alternating canonical (CMC) and grand canonical (GCMC) steps, i.e., by the movement of randomly chosen particle, and by the addition to or removal of particles from the system. Additions and removals were attempted randomly with a probability P, so the probability for a move of a randomly chosen particle was $1-2P$. The value $P \approx 0.15$ was used in most of our runs. A new configuration was first checked for a hard-core overlap. It was automatically rejected if overlap had been detected. In restricted geometry, the rejection applied to the moves or additions leading to an overlap of the moved or added particle with another molecule or with the boundaries of the confinement. After this check, the moves were accepted with the probability f_{ij} given by

$$f_{lj} = \min\{1, \exp[-\beta(u_j - u_i)]\} \tag{7}$$

with β having its usual meaning, $\beta = 1/kT$. The subscripts i and j denote the initial and the attempted configuration; $u_j - u_i$ is the change of the total configurational potential energy due to the particle move. Additions and removals were accepted with the probabilities[22]

$$\begin{aligned} f_{lj} &= \min\{1, r\}, \quad \text{for addition} \\ f_{ji} &= \min\{1, 1/r\}, \quad \text{for removal} \end{aligned} \tag{8}$$

where

$$r = \frac{\rho_b}{\rho_j} \exp[\beta(\mu_b^{ex} - u_j + u_i)] \tag{9}$$

In the above, the subscript ij denotes an increase and ji a decrease in the number of particles, i.e., $N_j = N_i + 1$. ρ_b and μ_b^{ex} are the mean number density and excess chemical potential of the bulk phase, and $u_j - u_i$ is the energy change due to the addition or deletion of a particle. The values for the excess chemical potential μ_b^{ex} for the prescribed (targeted) bulk densities were determined using iterative GCMC algorithm.[23]

The density profiles were determined from the average numbers of the particles found within the slices into which the elementary MC cell was subdivided. A typical duration of a GCMC run was about 2×10^6 trial moves per particle in the production calculation, and 5×10^5 moves per particle were needed to equilibrate the system. The allowed displacement of the moved particle was usually restricted to ascertain a move acceptance of about 60%.

2.3. Third-Order + Second-Order Perturbation DFT and Integral Equation Theory. The spirit of the third-order + second-order DFT lies in the fact that the long-ranged tail part $C_0^{(2)}{}_{\text{tail}}(r;\rho_b \cdots)$ of the bulk second-order direct correlation function (DCF) $C_0^{(2)}(r;\rho_b \cdots)$ only weakly depends on the density argument. Hence the functional perturbation expansion of the nonuniform first-order DCF $C^{(1)}(\rho_b \cdots)$) around the coexistence bulk density can be reliably truncated at the lowest order for the long-ranged part,[24] while for the short-ranged part truncation approximation at higher order[25] or other effective DFA[24,26] are needed. If the short-ranged part is treated by the third-order functional perturbation expansion approximation, then the resultant nonuniform first order DCF is given by[25]

$$C^{(1)}(\mathbf{r};[\rho] \cdots) = C_0^{(1)}(\rho_b \cdots) + \int d\mathbf{r}' [\rho(\mathbf{r}') - \rho_b] C_0^{(2)} \times (|\mathbf{r} - \mathbf{r}'|;\rho_b \cdots) + \frac{C_{0hc}^{(1)''}(\rho_b \cdots)}{2[C_{0hc}^{(1)'}(\rho_b \cdots)]^3} \int C_{0hc}^{(2)}(\mathbf{r}, \mathbf{r}'';\rho_b \cdots) \times \left[\int C_{0hc}^{(2)}(\mathbf{r}', \mathbf{r}'';\rho_b \cdots)(\rho(\mathbf{r}') - \rho_b) d\mathbf{r}'\right]^2 d\mathbf{r}'' \quad (10)$$

Throughout the text, superscript (n) denotes the corresponding n-order quantities; absence of the subscript 0 refers to nonuniform case, while the presence of the subscript 0 refers to the uniform case. It has been shown[25] that the physical coefficient $C_{0hc}^{(1)}{}''(\rho_b \cdots)/2[C_{0hc}^{(1)}{}'(\rho_b \cdots)]^3$ in the eq 10 can be used as an adjustable parameter denoted by λ. Then we finally have

$$C^{(1)}(\mathbf{r};[\rho] \cdots) = C_0^{(1)}(\rho_b \cdots) + \int d\mathbf{r}' [\rho(\mathbf{r}') - \rho_b] C_0^{(2)}(|\mathbf{r} - \mathbf{r}'|;\rho_b \cdots) + \lambda(\rho_b \cdots) \times \int C_{0hc}^{(2)}(\mathbf{r}, \mathbf{r}'';\rho_b \cdots)[\int C_{0hc}^{(2)}(\mathbf{r}', \mathbf{r}'';\rho_b \cdots) \times (\rho(\mathbf{r}') - \rho_b) d\mathbf{r}']^2 d\mathbf{r}'' \quad (11)$$

Combination of eq 11 with the DFT expression for the density profile of a single-component fluid

$$\rho(\mathbf{r}) = \rho_b \exp\{-\beta\varphi_{ext}(\mathbf{r}) + C^{(1)}(\mathbf{r};[\rho] \cdots) - C_0^{(1)}(\rho_b \cdots)\} \quad (12)$$

leads to the formalism enabling the calculation of the density profile $\rho(\mathbf{r})$ for the fluid subjected to diverse external fields. In eq 12, $\varphi_{ext}(\mathbf{r})$ is the external potential responsible for the formation of the inhomogeneous spatial density distribution $\rho(\mathbf{r})$. In these DFT calculations, the adjustable parameter λ is determined by a single hard-wall sum rule,[27] which claims the knowledge of the pressure of the coexistence bulk fluid. Because of possible small errors associated with the bulk pressure calculated using the pure theories, which can then interfere with the reliability of the judgment on the quality of the performance of the DFT approach, we utilize the simulation result for the pressure as an input, its value being related to the single hard-wall contact density $\rho(0.5\sigma)$ and is equal to $\rho(0.5\sigma)/\beta$. It means that the parameter λ is adjusted to the value ensuring the equality of the single hard-wall contact density predicted by the present DFT approach and that obtained by "exact" simulation method. Nevertheless, in practical cases one could also use the pressure based on the OZ integral equation. Although this would give rise to small quantitative errors in the calculations, it would certainly not affect the qualitative features of the final results.

Other external parameters imported in DFT calculation are the bulk second order DCF $C_0^{(2)}(r;\rho_b \cdots)$ and $C_{0hc}^{(2)}(r;\rho_b \cdots)$ of the coexistence bulk fluid with which the inhomogeneous fluid under consideration is in equilibrium. The $C_0^{(2)}(r;\rho_b \cdots)$ obtained by the numerical solution of the OZ integral equation is separated into the hard-core part $C_{0hc}^{(2)}(r;\rho_b \cdots)$ and the tail part $C_{0tail}^{(2)}(r;\rho_b \cdots)$:[24−26]

$$C_0^{(2)}(r;\rho_b \cdots) = C_{0hc}^{(2)}(r;\rho_b \cdots) + C_{0tail}^{(2)}(r;\rho_b \cdots) \quad (13)$$

with

$$C_{0hc}^{(2)}(r;\rho_b \cdots) = \begin{cases} C_0^{(2)}(r;\rho_b \cdots) & r < r_{cut} \\ 0 & r > r_{cut} \end{cases} \quad (14)$$

and

$$C_{0tail}^{(2)}(r;\rho_b \cdots) = \begin{cases} 0 & r < r_{cut} \\ C_0^{(2)}(r;\rho_b \cdots) & r > r_{cut} \end{cases} \quad (15)$$

Here r_{cut} specifies the distance at which the bulk second-order DCF is split into a hard-core part and a tail part. For the sample potential of our present interest, $g(r)$ is equal to zero for $r < \sigma$, which indicates strong dependence of the bulk second order DCF on the density argument at these distances. Hence the hard-sphere diameter σ should obviously be chosen as the value for r_{cut}.

A usual route used for obtaining the $C_0^{(2)}(r;\rho_b \cdots)$ is to solve the OZ integral equation

$$h(r) = C_0^{(2)}(r;\rho_b \cdots) + \rho_b \int d\mathbf{r}_1 h(\mathbf{r}_1) C_0^{(2)}(|\mathbf{r} - \mathbf{r}_1|;\rho_b \cdots) \quad (16)$$

along with an appropriate approximation for the bridge function $B(r)$ in the closure relation

$$h(r) + 1 = \exp\{-\beta u(r) + \gamma + B(r)\} \quad (17)$$

Here, $h(r) = g(r) - 1$ and $\gamma(r) = h - C_0^{(2)}(r;\rho_b \cdots)$ are the total and the indirect correlation functions, respectively. Although there exists a formal relationship between $B(r)$ and $g(r)$, it involves an infinite sum of highly connected diagrams, which render its utilization in practical calculation impossible. Further, a series expansion of the bridge function $B(r)$ in terms of higher order correlation functions has been also derived and is given by the expression

$$B(\mathbf{r}, \mathbf{r}') = \frac{\rho^2}{2} \int C_0^{(3)}(\mathbf{r}, \mathbf{r}_2, \mathbf{r}_3;\rho_b \cdots)[g(\mathbf{r}_2, \mathbf{r}') - 1] \times [g(\mathbf{r}_3, \mathbf{r}') - 1] d\mathbf{r}_2 d\mathbf{r}_3 + \cdots \quad (18)$$

However, the convergence of this series is notoriously slow, and, in addition, it introduces new unknown functions. Hence this series expansion actually does not help to formulate accurate bridge function approximation. For single-component fluids with the usual interparticle potentials, much research work has been done to create appropriate approximations for the bridge function. It is well-known that the consistency between different thermodynamic routes plays a key role in improving the accuracy of the predicted $g(r)$. The thermodynamic consistency condition usually employed for the formulation of the satisfactory approximation for the bridge function $B(r)$ is the so-called global self-consistency criterion, which claims the equality of the results for the pressure obtained via the virial route, P^v, and via the compressibility route, P^c, respectively. As the calculation of the pressure P^c includes integration of the inverse isothermal compressibility along a density path, the implementation of the global self-consistency criterion would demand intensive numerical computation. For this reason, instead of utilizing this criterion, one usually resorts to the so-called local thermody-

namic self-consistency condition, which imposes equality of the inverse isothermal compressibility $\chi_T^{v-1} = \partial\beta P^v/\partial\rho$ obtained by deriving the virial pressure P^v with respective to the bulk density and the same quantity $\chi_T^{c-1} = \partial\beta P^c/\partial\rho$ obtained by the compressibility route:

$$\frac{\beta P^v}{\rho} = 1 - \frac{\beta\rho_b}{6}\int_0^\infty \mathrm{d}r\, 4\pi r^3 \frac{\mathrm{d}u(r)}{\mathrm{d}r} g(r) \tag{19}$$

$$\frac{\beta\,\partial P^c}{\partial\rho_b} = 1 - \rho_b \int \mathrm{d}\mathbf{r}\, C_0^{(2)}(\mathbf{r};\rho_b \cdots) \tag{20}$$

In the present work we employ the modified hypernetted chain (MHNC) approximation[28] for the bridge function $B(r)$, which needs the hard-sphere bridge function as an input. In this investigation, the following approximate hard-sphere bridge function is employed:[29]

$$B_{hs}(r) = \begin{cases} \ln(y_{hs}(r)) + 1 + C_{0hs}^{(2)}(r) & r < \sigma \\ \ln(g_{hs}(r)) + C_{0hs}^{(2)}(r) + 1 - g_{hs}(r) & r > \sigma \end{cases} \tag{21}$$

Individual terms in eq 21 are given by simulation data-fitting formulas of different authors, i.e., of Groot, van der Erden, and Faber,[36] Balance and Speedy,[37] and Verlet and Weis.[38] This function is therefore denoted as GvEF-BS-VW hard-sphere bridge function, as proposed by one of the authors of this study in the work of ref 29. It has been shown that a combination of the GvEF-BS-VW hard-sphere bridge function and the MHNC approximation for the OZ integral equation performs very well for the Lennard-Jones fluid. The MHNC approximation is associated with an adjustable parameter, i.e. the effective hard-sphere diameter whose value we specify by the local thermodynamic self-consistency condition. For the details about the numerical procedure, we refer the reader to ref 29. Upon numerical solution of the OZ integral equation, one obtains the radial distribution function $g(r)$, which is compared with the corresponding simulation data, and the DCF $C_0^{(2)}(r;\rho_b \cdots)$, which is used as an input for the third order + second order perturbation DFT.

In our previous publications[25,30,31] it has been shown that the third-order + second-order perturbation DFT is physically reliable and quantitatively sufficiently accurate for some model fluids such as the HCAY[25,30] and LJ[31] fluids only on condition of high accuracy of the bulk $C_0^{(2)}(r;\rho_b\cdots)$.

3. Numerical Results and Discussion

In the following we present the theoretical and simulation results for the homogeneous and inhomogeneous structure of the fluid comprising the particles interacting via the effective potential given by eqs 1 and 2. We perform calculations at two sets of the potential parameters: (I) $b = 1.1$, $\alpha = 0.55$, $k_s = 12$, $n = 3$, $\varepsilon_b = 1.0$, and (II) $b = 1.1$, $\alpha = 0.8$, $k_s = 16$, $n = 4$, $\varepsilon_b = 0.4$. The appropriate choice of the temperature of the coexisting bulk fluid is based on the knowledge of the critical value T_c. The reduced critical temperatures $T_c^* = kT_c/\varepsilon$ at individual sets of potential parameters are determined by means of a third-order thermodynamic perturbation theory (TPT),[32] which has been recently proposed by one of the authors of this work. This theory has been shown to perform well for various potentials, among others also for the sample potential of the present interest, for which the third-order TPT performs excellently for the prediction of the thermodynamic properties.[33] We therefore believe that the critical temperatures determined by this theory should be close to the exact values. For the above parameter sets I and II, the corresponding values for the reduced critical temperatures T_c^* are 0.375 and 0.3, respectively.

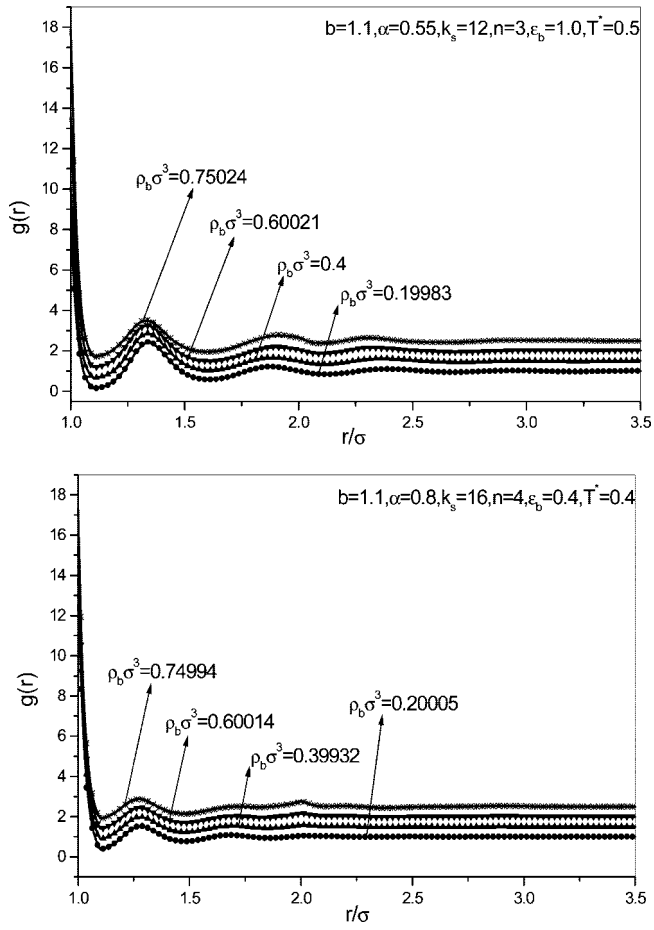

Figure 2. Theoretical (lines) and simulation (symbols) results for the bulk radial distribution function of the fluid at two parameter sets (I) and (II) as described in the caption of Figure 1 and at different densities.

Figure 1 displays the potential function, which show oscillatory decaying behavior at the distances $r > b\sigma$. In Figure 2 we present the radial distribution function (RDF) of the bulk fluid for the individual sets of potential parameters and at different densities, whereas Figures 3−10 show the density profiles of the same fluid: (i) at a single hard wall (Figures 3 and 4), (ii) in the planar gap of width $L = 4\sigma$ (Figures 5 and 6), (iii) in the spherical cavity of radius $R = 4\sigma$ (Figures 7 and 8), and (iv) near a hard spherical particle of radius $R = 0.7\sigma$ (Figures 9 and 10). For the sake of clarity, the majority of these figures are subdivided into two or three parts, which successively illustrate the effect of increase in the bulk density at constant values of potential parameters.

Bulk RDFs shown in Figure 2 are computed by solving the OZ integral equation along with the MHNC approximation[28] in combination with the recently proposed hard sphere bridge function approximation.[29] As in narrow domain close to contact distances the potential (Figure 1) is attractive, this gives rise to high contact values of $g(r)$ and deep minima at the distances slightly exceeding the contact values. These minima stem from the exclusion volume effect of the molecular layer firmly attached to the central particle, and, in addition, from the fact that the linear attractive part in the potential function at $r < b\sigma$ is followed by the repulsive part of the first oscillating cycle. At higher distances the shape of $g(r)$ is oscillatory due to the layering structure of the fluid. It is interesting to observe that

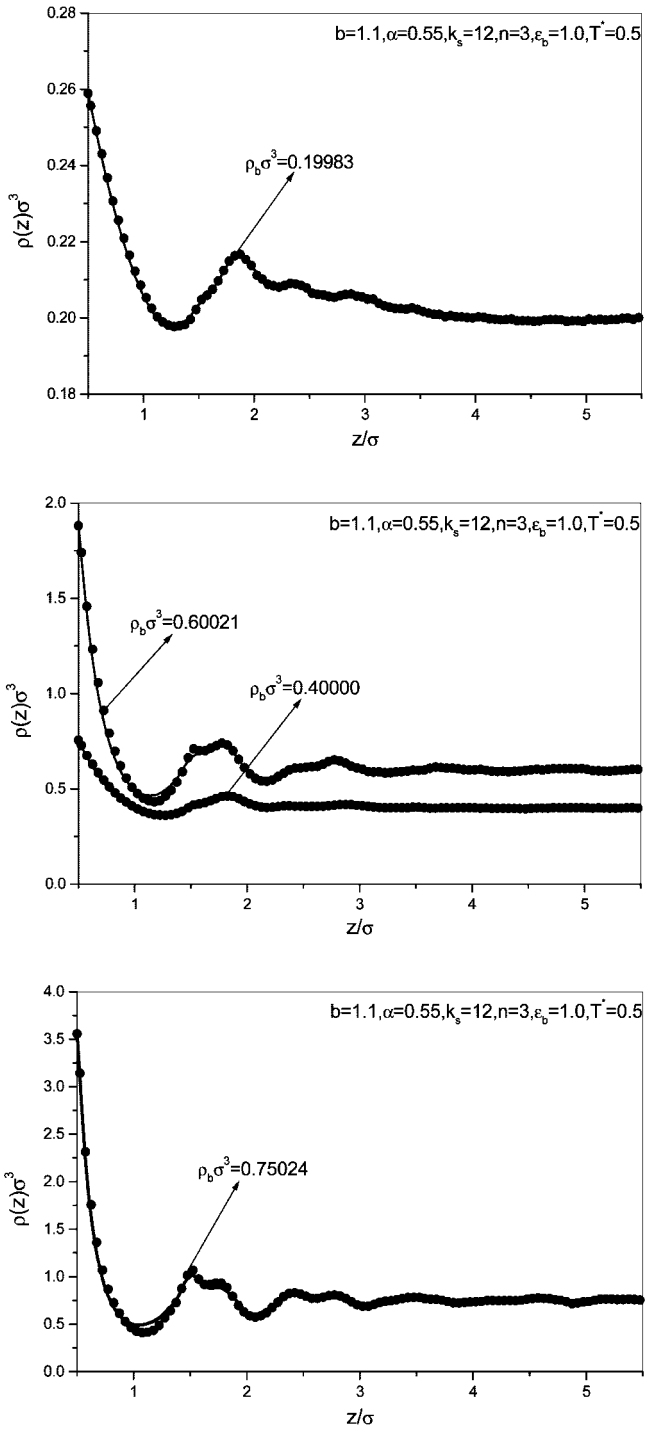

Figure 3. Theoretical (lines) and simulation (symbols) results for the density profiles of the fluid with the potential parameter set (I) $b = 1.1$, $\alpha = 0.55$, $k_s = 12$, $n = 3$, $\varepsilon_b = 1.0$ near a single hard wall at the reduced temperature $T^* = 0.5$ and at different values of the bulk density.

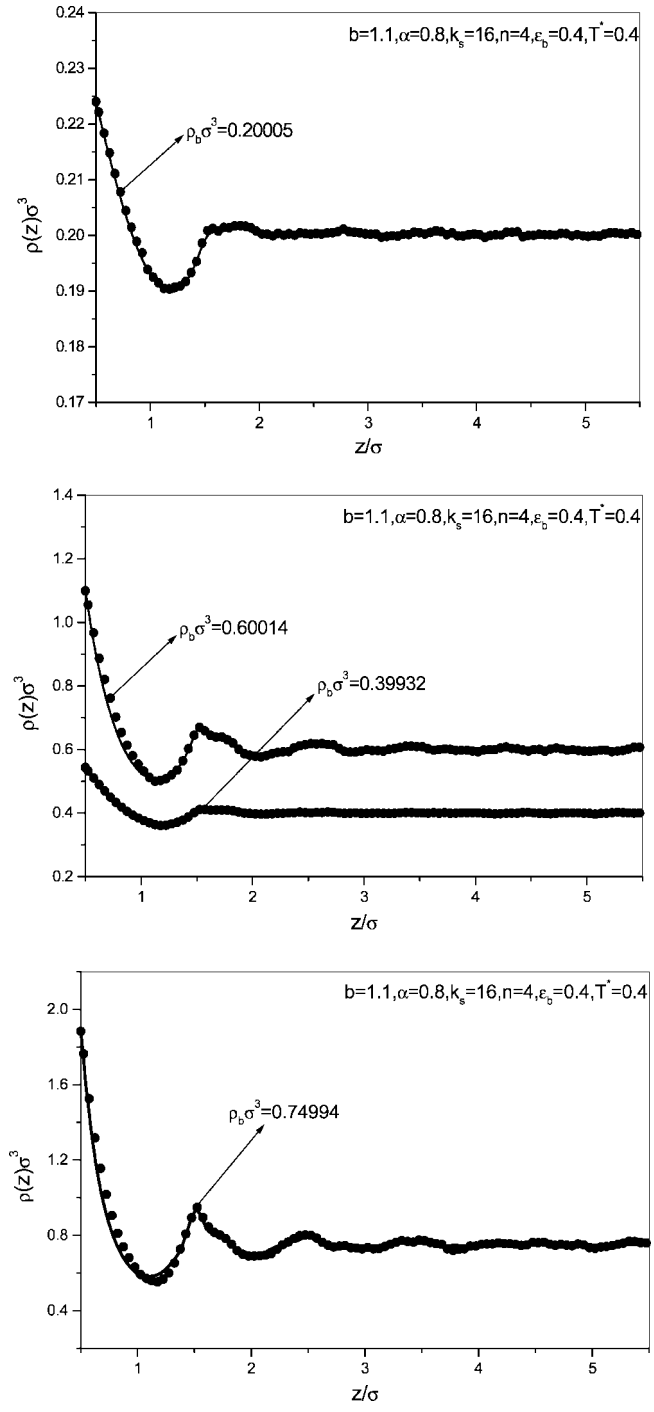

Figure 4. Same as Figure 3 but for the parameter set (II) $b = 1.1$, $\alpha = 0.8$, $k_s = 16$, $n = 4$, $\varepsilon_b = 0.4$, and the reduced temperature $T^* = 0.4$.

the period of oscillations approximately coincides with that in the potential function, i.e., the minima in $g(r)$ approximately coincide with the maxima (repulsion) in the oscillatory potential function and vice versa. For example, we can imagine the spatial arrangement of particles $i-j-k\cdots$ as such that the distances between individual pairs fall in qualitatively different (attractive or repulsive) range of the oscillatory potential. In any case, irrespective of the actual interactions between $j-k\cdots$ particles, they feel some mixed influence of the central particle i. The resulting structure therefore results from such competitive interactions. Rapid look at the computed RDFs indicates excellent agreement between the results obtained by the approximate integral equation theory and simulation data. The same holds also for some thermodynamic data gathered in Table 1. In all cases the agreement between the theoretical and simulation data for the excess internal energy U^{ex}/NkT and the compressibility factor $Z = \beta P/\rho_b$ is excellent to very good, depending on the density of the system.

The results for the inhomogeneous structure of the fluid displayed in Figures 3−10 show the structural features characteristic for the behavior of fluids at the interfaces and in confined systems.

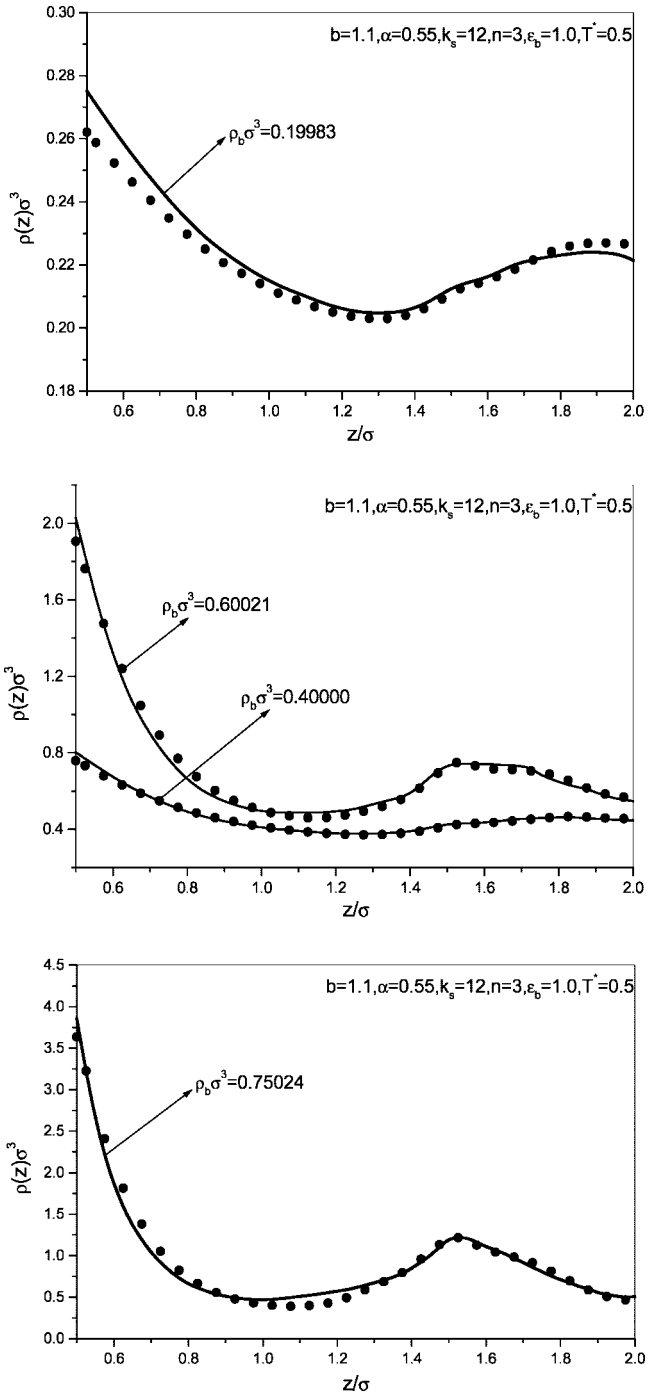

Figure 5. Theoretical (lines) and simulation (symbols) results for the single-wall density profiles of the fluid with the potential parameter set (I) $b = 1.1$, $\alpha = 0.55$, $k_s = 12$, $n = 3$, $\varepsilon_b = 1.0$ in a planar gap of width $L = 4\sigma$ at the reduced temperature $T^* = 0.5$ and at different values of the bulk density.

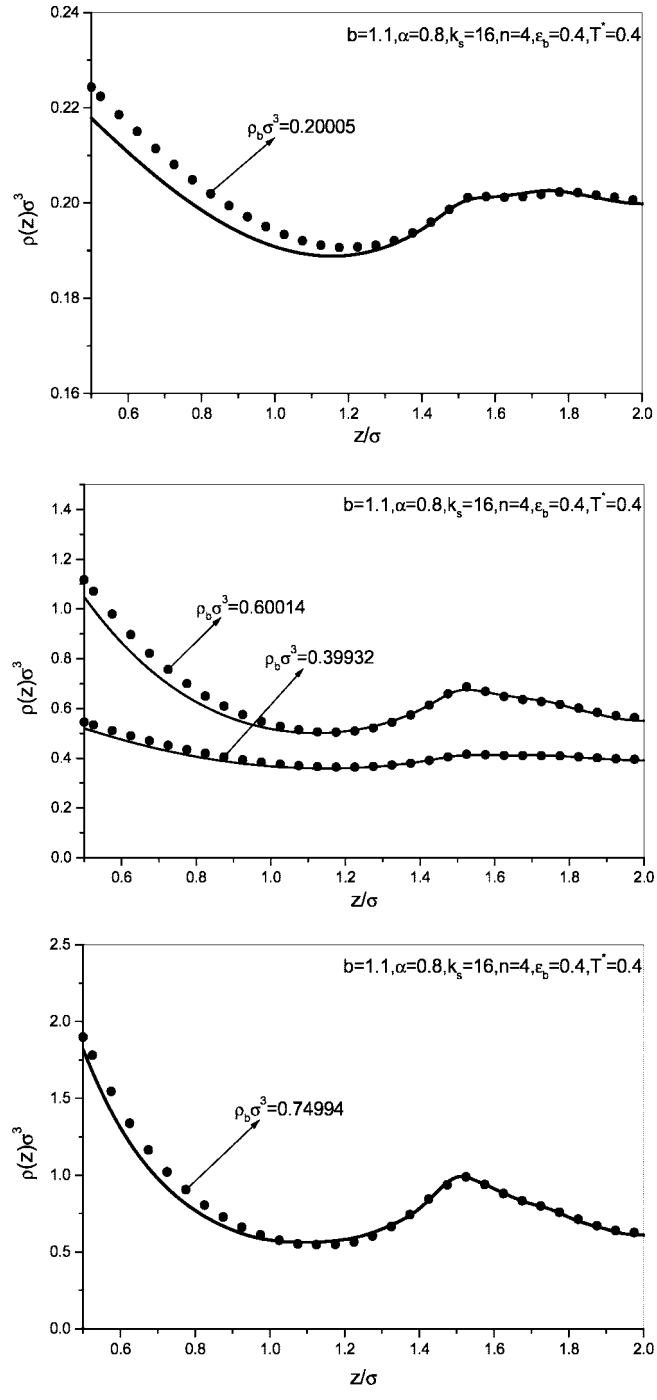

Figure 6. Same as Figure 5 but for the parameter set (II) $b = 1.1$, $\alpha = 0.8$, $k_s = 16$, $n = 4$, $\varepsilon_b = 0.4$, and the reduced temperature $T^* = 0.4$.

The course of the density profiles that characterize spatial inhomogeneities depends on the specific nature of the fluid−fluid and the wall−fluid interactions, and on the degree and geometry of confinement. When an inhomogeneous structure of the fluid stems from the presence of a single wall, flat density profiles $\rho(x) = \rho_b$ are restored at sufficient distances from the wall, irrespective of the specific nature of the intermolecular potential of interactions. Upon approaching the wall these interactions begin to compete with steric effects. This competition, of course, is now strongly dependent on the particular intermolecular potential and in addition, on the temperature of the system. In any case, the interparticle interactions have a stronger influence on the structure of the fluid at lower temperatures. As the strongly attractive molecules have a better chance for mutual attraction at sufficient distances from the wall(s) or outside the confined system, they are driven away from the hard obstacles or toward the center of the micro-objects with restricted geometry. Of course, just the opposite behavior has been observed for the molecules interacting through purely repulsive interaction potential. Clearly, strongly repulsive molecules try to avoid each other and as such they prefer the regions adjacent to the walls of the confinement. Such molecules are therefore accumulated next to the walls to a greater extent than those incorporating some attractive interactions, thus giving

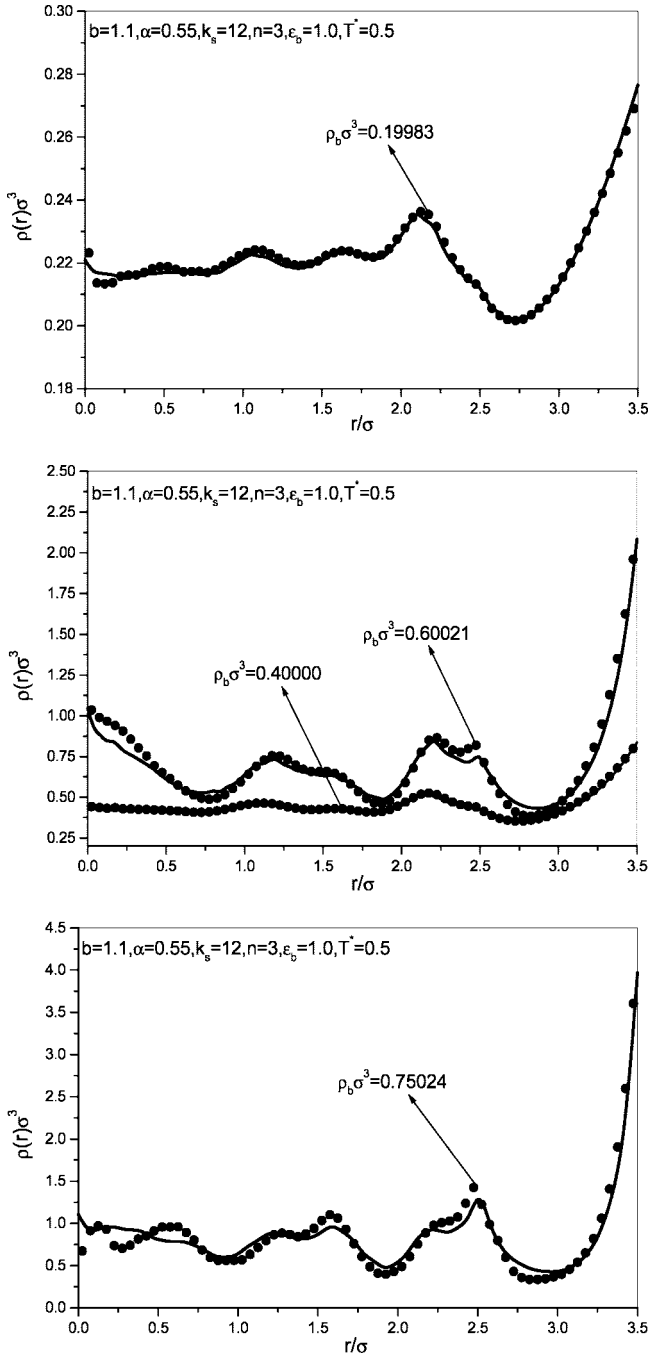

Figure 7. Theoretical (lines) and simulation (symbols) results for the density profiles of the fluid with the potential parameter set (I) $b = 1.1$, $\alpha = 0.55$, $k_s = 12$, $n = 3$, $\varepsilon_b = 1.0$ in a spherical cavity of radius $R = 4\sigma$ at the reduced temperature $T^* = 0.5$ and at different values of the bulk density.

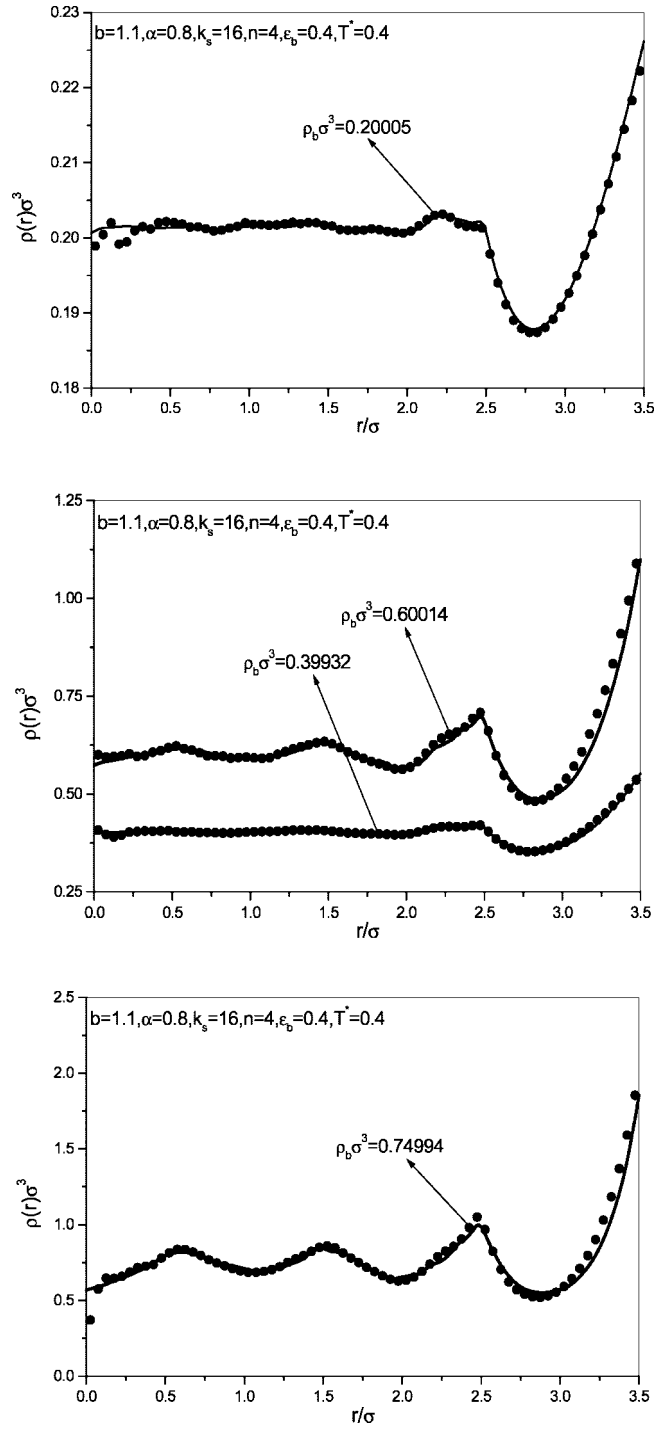

Figure 8. Same as Figure 7 but for the parameter set (II) $b = 1.1$, $\alpha = 0.8$, $k_s = 16$, $n = 4$, $\varepsilon_b = 0.4$, and the reduced temperature $T^* = 0.4$.

rise to more pronounced packing effects leading to more distinct layering structure and higher wall−fluid contact density of the fluid with repulsive particles. As mentioned above, the role of the interparticle interactions strengthens with reducing the temperature. For this reason, lowering the temperature causes a decrease of the contact density and weaker oscillations in the density near the walls in the case of the model fluids with attractive molecules. Again, just the opposite holds for the fluid comprising the particles interacting via purely repulsive potential function (e.g., hard core repulsive Yukawa fluid). In summary, imposing the qualitatively different interactions (attractive or repulsive) to the molecules of the fluid gives rise to qualitatively different redistributions of the molecules inside the confined system, leading to thermodynamically the most favorable structures in both cases. In the case of the model fluid of our present interest, which incorporates both repulsive and attractive interactions in the oscillating potential function, one meets with a combination of all these effects. The resulting density profiles of confined fluid thus show the shapes arising from the complex interplay among the steric effects and the alternating repulsive and attractive parts of the effective potential. One can observe more or less sharp peak evolving at the distance $z = 1.5\sigma$ from the walls. This peak corresponds to the configuration of two successive molecular layers—the first comprising the molecules accumulated adjacent to the walls, and the second with the

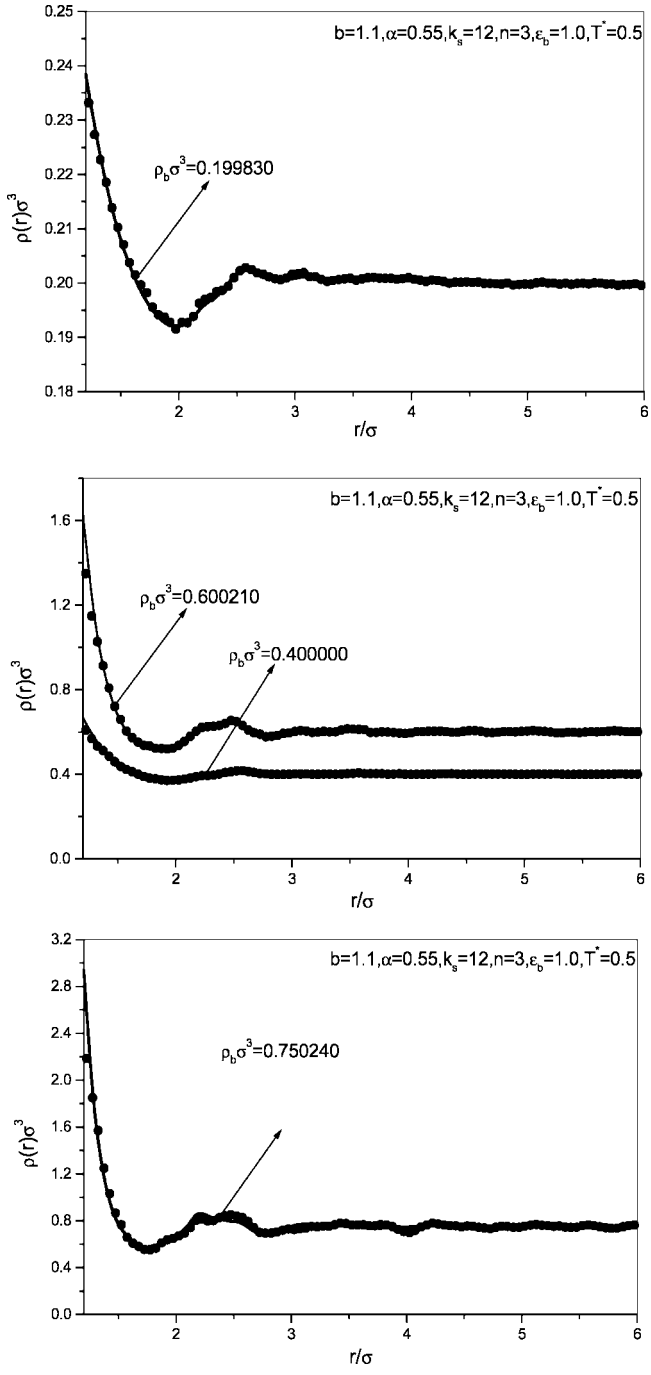

Figure 9. Theoretical (lines) and simulation (symbols) results for the density profiles of the fluid with the potential parameter set (I) $b = 1.1$, $\alpha = 0.55$, $k_s = 12$, $n = 3$, $\varepsilon_b = 1.0$ near a hard spherical particle of radius $R = 0.7\sigma$ at the reduced temperature $T^* = 0.5$ and at different values of the bulk density.

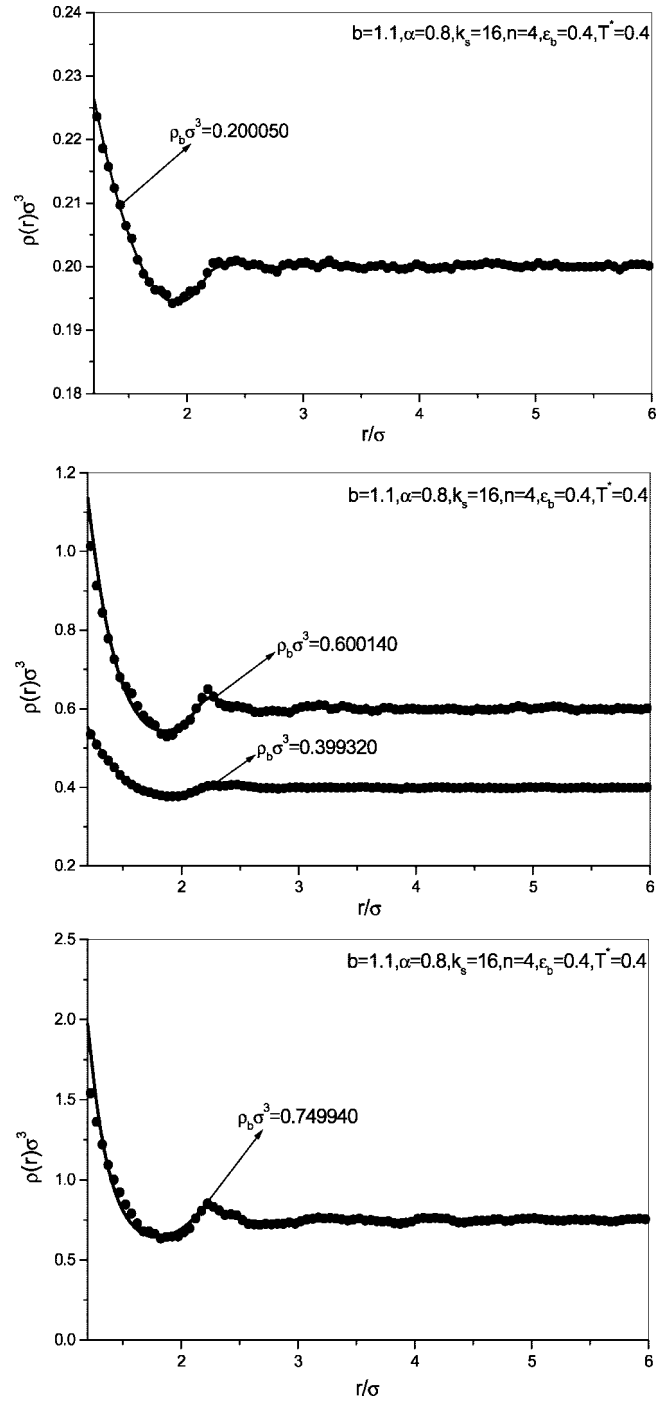

Figure 10. Same as Figure 9 but for the parameter set (II) $b = 1.1$, $\alpha = 0.8$, $k_s = 16$, $n = 4$, $\varepsilon_b = 0.4$, and the reduced temperature $T^* = 0.4$.

molecules strongly attached by the first layer. At larger distances one sees the layering structure, the actual shape of the density profiles being governed by alternating repulsive and attractive intermolecular potential. This structure is not typical as found for the fluids with the molecules interacting via monotonically changing attractive or repulsive (tail) potential. In the present case, successive molecules may feel qualitatively different (repulsive or attractive) interaction with their surrounding molecules. For this reason, as stated above in the discussion of the bulk structure, the density profiles show somewhat peculiar shapes also at larger distances from the walls. As stated above, the strongly attractive molecules are driven away from the hard obstacles, leading to energetically more favorable configurations. Accordingly, it may look surprising that no depletion of particles at contact wall(s)−fluid distances is observed. Although the intermolecular potential of interaction is attractive at short distances the particles accumulate near the hard objects in all cases. However, the resulting inhomogeneous structure follows from the complex interplay between the attractive and repulsive parts of the interaction potential. Therefore, a depletion effect could actually be expected at the values of parameters corresponding to much stronger attraction acting in the narrow range of the intermolecular distances slightly exceeding the contact value. A careful inspection of the results for the local structures of the fluid in different inhomogeneous systems indicates fair

TABLE 1: Excess Internal Energy U^{ex}/NkT and the Compressibility Factor $Z = \beta P/\rho_b$ of the Fluid at Two Sets of the Potential Parameters: (I) $b = 1.1$, $\alpha = 0.55$, $k_s = 12$, $n = 3$, $\varepsilon_b = 1.0$ and (II) $b = 1.1$, $\alpha = 0.8$, $k_s = 16$, $n = 4$, $\varepsilon_b = 0.4$, Determined by the OZ Equation and from the GCEMC Simulations[a]

		U^{ex}/NkT		$Z = \beta P/\rho_b$	
	$\rho_b\sigma^3$	theory	GCEMC	theory	GCEMC
set I	0.19983	−0.7123	−0.7152	1.2985	1.2957
	0.40000	−1.4821	−1.4920	1.9106	1.8878
	0.60021	−2.4207	−2.4292	3.2021	3.1350
	0.75024	−3.2278	−3.2603	4.8924	4.7404
set II	0.20005	−0.8027	−0.8048	1.1217	1.1198
	0.39932	−1.6604	−1.6730	1.3664	1.3612
	0.60014	−2.6574	−2.6956	1.8673	1.8315
	0.74994	−3.5700	−3.6208	2.6052	2.5110

[a] The MC pressure is obtained by the simulation of the fluid confined in the gap of width $L = 21\sigma$ applying the contact theorem $\beta P = \rho(0.5\sigma)$.

to very good agreement between the DFT predictions and simulation data. As expected, the accuracy of the pure theory depends on the expressiveness of the "inhomogeneity" of the system. For this reason, as expected, the theory does the best job in the case of a single hard wall (Figures 3 and 4) as a source of the external field, whereas slight to somewhat higher discrepancies between the DFT and GCMC results are observed in the case of confined systems. However, also in most of these cases almost quantitative agreement between the results of both methods is observed, the exception being the DFT density profiles referring to the highest density of the fluid confined in the spherical cavity (Figure 7). Of course, an excellent agreement between the DFT and GCMC density profiles near a single hard wall stem also from the fact that the adjustable parameter λ is determined by the single hard wall sum rule, where this parameter is adjusted to the value ensuring the equality of the DFT and GCMC contact densities. We can therefore conclude that the third-order + second-order perturbation DFT approach represents an adequate theoretical tool for the investigations of the inhomogeneous structure of the fluid comprising the molecules interacting through an effective potential, which incorporates interaction terms typical for the modeling of complex fluids.

The numerical implementation of the present third-order + second-order perturbation DFT requires the knowledge of the physical parameter $\lambda(\rho_b \cdots)$. This parameter was determined by a single hard-wall sum rule, which claims the knowledge of the pressure of the coexistence bulk fluid. To avoid the possible interference on the judgment on the quality of the performance of the DFT approach from the possible small errors associated with the bulk pressure calculated using the approximate pure theories, we employed the simulated pressure in the present calculations. In actual calculation, just as we utilized the $C_0^{(2)}(r;\rho_b \cdots)$ from the OZ integral equation as an input to switch the procedure, we could also use the virial pressure P^v of eq 19 obtained by the numerical solution of the OZ integral equation. In Table 1 one can see that the bulk pressure calculated by the pure theory and that resulting from the simulation agree within a few percent. This means, that the final outcome would be only slightly sensitive to the use of either value for the bulk pressure.

4. Conclusions

In the present work, we have surprisingly found that the well-established approximate theories applicable for the study of ordinary neutral atomic fluids with the particles interacting through Lennard-Jones like potentials perform well also for the system of particles interacting through the effective potentials useful for the modeling of complex fluids. The essential point of the modified hypernetted chain (MHNC) approximation is that the non-hard-sphere fluid can be mapped onto the hard-sphere fluid with some effective diameter. The key for a successful performance of the MHNC approximation is therefore the presence of a highly repulsive core in the interparticle potentials. The main effect of the interaction tail is then to perturb the structures originating from the highly repulsive core interaction. The present effective sample potential also includes the highly repulsive hard-sphere core as an ingredient, which is exactly the reason for a successful performance of the MHNC approximation. On the other hand, the reliability of the third-order + second-order perturbation DFT critically depends on the weak dependence of the tail part of bulk second-order DCF on the density argument, which also originates from the presence of the highly repulsive hard core in the potential functions. This explains why this DFT approximation performs well for the effective potential model fluid subjected to various external fields. The present investigation further indicates that the van der Waals picture, which declares that the interaction tail constitutes only a small perturbation to the hard-sphere fluid, applies not only for the ordinary neutral atomic potential but also for the effective potentials with a highly repulsive core. The only premise condition, which enables the van der Waals picture applicable also for the effective potentials, is the presence of a highly repulsive core in the potential function. Then, in particular, the van der Waals picture also applies for the inhomogeneous cases.

A naturally arising problem is—to what extent does the the van der Waals picture apply for the finite repulsive core? Such cases are actually popular in the modeling of complex fluids and include, for example, the so-called "Gaussian core model" of Stillinger,[34] which models the effective interaction potential between two polymer coil colloids in a good solvent, and the penetrable sphere model, which was first proposed by Marquest and Witten[35] for the micellar solutions. As in the systems dominated by the bounded potentials the exclusion volume effect is rather small, it would be an interesting topic how to modify these well-established approximations and the van der Waals methodology to make them applicable for the study of such systems. We will report these investigations in the near future.

Acknowledgment. The authors are thankful for the financial support of the Slovenian Research Agency (Grants Nos. P1-0201 and J1-6653) and the National Natural Science Foundation of China (Grant No. 20673150).

References and Notes

(1) Martynov, G. A. *Fundamental Theory of Liquids. Method of Distribution Functions*; Adam Hilger: Bristol, UK, 1992.
(2) Hansen, J. P.; McDonald, I. R. *Theory of Simple Liquids*; Academic Press: London, 1986.
(3) Henderson, D. *Fundamentals of Inhomogeneous Fluids*; Marcel Dekker: New York, 1992.
(4) Barker, J. A.; Henderson, D. *Rev. Mod. Phys.* **1976**, *48*, 587.
(5) Zhou, S. *Phys. Rev. E* **2008**, *77*, 041110.
(6) Abramo, M. C.; Caccamo, C. *Phys. Lett. A* **1992**, *166*, 70.
(7) Willenbacher, N.; Oelschlaeger, C. *Curr. Opin. Colloid Interface Sci.* **2007**, *12*, 43.
(8) Likos, C. N. *Phys. Rep.* **2001**, *348*, 267.
(9) Zhou, S. *Commun. Theor. Phys. (Beijing, China)* **2005**, *44*, 365.
(10) Gazzillo, D.; Giacometti, A.; Fantoni, R.; Sollich, P. *Phys. Rev. E* **2006**, *74*, 051407.
(11) Gutsche, C.; Keyser, U. F.; Kegler, K.; Kremer, F.; Linse, P. *Phys. Rev. E* **2007**, *76*, 031403.

(12) Shinto, H.; Minoru, M.; Higashitani, K. *J. Colloid Interface Sci.* **1999**, *209*, 79.
(13) Louis, A. A.; Allahyarov, E.; Lowen, H.; Roth, R. *Phys. Rev. E* **2002**, *65*, 061407.
(14) Richetti, P.; Kékicheff, P. *Phys. Rev. Lett.* **1992**, *68*, 1951.
(15) Roth, R.; Kinoshita, M. *J. Chem. Phys.* **2006**, *125*, 084910.
(16) Wax, J. F.; Albaki, R.; Bretonnet, J. L. *Phys. Rev. B.* **2000**, *62*, 14818.
(17) Moriarty, J. A.; Widom, M. *Phys. Rev. B* **1997**, *56*, 7905.
(18) Largo, J.; Wilding, N. B. *Phys. Rev. E* **2006**, *73*, 036115.
(19) Velasco, E.; Navascués, G.; Mederos, L. *Phys. Rev. E* **1999**, *60*, 3158.
(20) Asakura, S.; Oosawa, F. *J. Chem. Phys.* **1954**, *22*, 1255.
(21) Götzelmann, B.; Evans, R.; Dietrich, S. *Phys. Rev. E* **1998**, *57*, 6785.
(22) Frenkel, D.; Smit, B. *Understanding Molecular Simulation*; Academic Press: Boston, MA, 1996.
(23) Malasics, A.; Gillespie, D.; Boda, D. *J. Chem. Phys.* **2008**, *128*, 124102.
(24) Zhou, S. *Phys. Rev. E* **2003**, *68*, 061201.
(25) Zhou, S. *Commun. Theor. Phys. (Beijing, China)* **2003**, *40*, 721.
(26) Zhou, S. *J. Chem. Phys.* **2004**, *121*, 895.
(27) Henderson, J. R. In *Fundamentals of Inhomogeneous Fluids*; Henderson, D., Ed.; M. Dekker: New York, 1992.
(28) Rosenfeld, Y.; Ashcroft, N. W. *Phys. Rev. A* **1979**, *20*, 1208.
(29) Zhou, S. *Theor. Chim. Acta* **2007**, *117*, 555.
(30) Zhou, S.; Jamnik, A. *J. Chem. Phys.* **2005**, *122*, 064503.
(31) Zhou, S.; Jamnik, A. *J. Chem. Phys.* **2005**, *123*, 124708.
(32) Zhou, S. *Phys. Rev. E.* **2006**, *74*, 031119.
(33) Zhou, S.; Solana, J. R. *Phys. Rev. E*., in press.
(34) Stillinger, F. H. *J. Chem. Phys.* **1976**, *65*, 3968.
(35) Marquest, C.; Witten, T. A. *J. Phys. (Paris)* **1989**, *50*, 1267.
(36) Groot, R. D.; van der Eerden, J. P.; Faber, N. M. *J. Chem. Phys.* **1987**, *87*, 2263.
(37) Ballance, J. A.; Speedy, R. J. *Mol. Phys.* **1985**, *54*, 1035.
(38) Verlet, L.; Weis, J.-J. *Phys. Rev. A.* **1972**, *5*, 939.

JP804852Y